Weierstraß-Institut

für Angewandte Analysis und Stochastik

Leibniz-Institut im Forschungsverbund Berlin e. V.

Mode-locking in systems of globally coupled phase oscillators

Sebastian Eydam, Matthias Wolfrum

Weierstrass Institute
Mohrenstr. 39
10117 Berlin
Germany
E-Mail: sebastian.eydam@wias-berlin.de
        matthias.wolfrum@wias-berlin.de

Mode-locking in systems of globally coupled phase oscillators

Sebastian Eydam, Matthias Wolfrum

Abstract

We investigate the dynamics of a Kuramoto-type system of globally coupled phase oscillators with equidistant natural frequencies and a coupling strength below the synchronization threshold. It turns out that in such cases one can observe a stable regime of sharp pulses in the mean field amplitude with a pulsation frequency given by spacing of the natural frequencies. This resembles a process known as mode-locking in lasers and relies on the emergence of a phase relation induced by the nonlinear coupling. We discuss the role of the first and second harmonic in the phase-interaction function for the stability of the pulsations and present various bifurcating dynamical regimes such as periodically and chaotically modulated mode-locking, transitions to phase turbulence and intermittency. Moreover, we study the role of the system size and show that in certain cases one can observe type-II supertransients, where the system reaches the globally stable mode-locking solution only after an exponentially long transient of phase turbulence.

Starting from the pioneering work of Kuramoto [1], systems of coupled phase oscillators became a fundamental paradigm for the study of the collective dynamics in coupled oscillatory systems. According to the classical theory [1, 2], a large system of oscillators with heterogeneous natural frequencies under the influence of a sufficiently strong all-to-all attractive coupling undergoes a transition from a disordered state of phase turbulence to a stable regime of partial synchrony.

In this paper, we study the specific case of equidistant natural frequencies [3, 4, 5], sometimes called *frequency comb*. It turns out that in this case already for a coupling strength below the Kuramoto threshold of transition to partial synchrony, there can appear stable states of collective order, which are characterized by sharp pulsations in the mean field amplitude occurring at a frequency close to the spacing of the natural frequencies. Due to their similarity to the regime of mode-locking in lasers [6, 7, 8], we call them mode-locked-solutions (MLSs), even though there can be made no direct connection between the physical mechanisms leading to mode-locking in laser devices and the global mean field coupling in our Kuramoto-type model. However the basic mechanism of establishing a phase relation between all modes without synchronizing them seems to be the same. Hence, the simple phase oscillator model can serve as a fundamental paradigm to understand in more detail the basic mechanisms of this fundamental dynamical process. Moreover, in [9] it has been pointed out, how the phase dynamics of a specific optical system can be related to a, however in this case more complicated, phase-oscillator model.

The paper is organized as follows: In Sec. 1 the model and its mean field formulation are introduced. The notion of MLSs and the key quantities that can be used to characterize them follow in Sec. 2. In Sec. 3 numerical schemes are introduced. The mode-locking mechanism is discussed in detail in Sec. 4. In Sec. 5 the dependence of chaotic transients that precede MLSs is studied in dependance of the system size and the shape of the interaction function. In Sec. 6 the parameter space is surveyed and various types of solutions are discussed. We summarize and discuss our findings in Sec. 7.

1 The Kuramoto-model on a frequency comb

Our basic system consist of globally coupled phase oscillators

$$\dot{\theta}_k = \omega_k + \frac{K}{N} \sum_{j=-n}^{n} \left[\gamma \sin(\theta_j - \theta_k) + (1 - \gamma) \sin(2(\theta_j - \theta_k)) \right], \tag{1}$$

where $k \in \{-n, \dots, n\}$ is the oscillator index, $N = 2n + 1$ is the number of oscillators, and K the coupling strength. The natural frequencies ω_k are given as a frequency comb

$$\omega_k = k\,\Delta\omega \tag{2}$$

with spacing $\Delta\omega$. In contrast to the classical Kuramoto-model, we are using an attracting phase interaction function including both first and second harmonic terms [10], balanced by the additional parameter $\gamma \in [0, 1]$. Normalizing the maximal natural frequency $\omega_n = 1$, such that $\omega_k \in [-1, 1]$, we obtain the spacing of the natural frequencies to be $\Delta\omega = 2/(N - 1)$. For convenience, we assume the number of oscillators $N = 2n + 1$ to be odd and the frequency comb to be symmetric with respect to $\omega_0 = 0$.

As in [9, 11], there is an equivariance of the system with respect to the transformation

$$\sigma : \theta_k \to -\theta_{-k} \quad \text{for all } k \in \{-n, \dots, n\}, \tag{3}$$

allowing for solutions with the symmetry

$$\phi_k(t) = -\phi_{-k}(t) \quad \text{for all } k \in \{1, \dots, n\}, \tag{4}$$

where $\phi_k = \theta_k - \theta_0$ is the phase difference with respect to the central mode. The distance to the symmetry invariant subspace can be monitored by the quantity

$$\chi = \frac{1}{n} \sqrt{\sum_{k=1}^{n} (\phi_k + \phi_{-k})^2}, \tag{5}$$

to detect possible symmetry breaking.

Due to our specific choice of the interaction function, one can rewrite (1) using the first and the second complex order parameter [12]

$$\eta_q(t) = R_q(t) e^{i\Psi_q(t)} = \frac{1}{N} \sum_{k=-n}^{n} e^{iq\theta_k(t)}, \quad q \in \{1, 2\} \tag{6}$$

and obtain

$$\dot{\theta}_k = \omega_k - K \left[R_1 \gamma \sin(\theta_k - \Psi_1) + R_2(1 - \gamma) \sin(2\theta_k - \Psi_2) \right]. \tag{7}$$

The quantities R_q and Ψ_q characterize the collective behavior of the system. While $R_1(t)$ quantifies the degree of total phase synchronization, $R_2(t)$ is a measure of two cluster emergence [1, 13].

2 The notion of mode-locking for phase oscillators

For a given dynamical regime of the system, we can define the average effective frequencies

$$\Omega_k := \lim_{t \to \infty} \frac{1}{t} \int_0^t \dot{\theta}_k(\tau) d\tau = \lim_{t \to \infty} \frac{\theta_k(t) - \theta_k(0)}{t}, \tag{8}$$

for $k \in \{-n, \dots, n\}$ and relative frequencies

$$\Omega_{k,j} := \Omega_k - \Omega_j \quad \text{for all } k \neq j. \tag{9}$$

For a mode-locked solution (MLS), we require that the effective frequencies form again a frequency comb, i.e

$$\Omega_{k,k+1} = \Delta\Omega \quad \text{for all } k \in \{-n, \dots, n-1\}. \tag{10}$$

The second property of MLSs is the formation of large pulses $R_1 \approx 1$ in the order parameter through a self organized recurring phase relation among the oscillators. The formation of the pulse is due to the fact that after each period of $T = 2\pi/\Delta\Omega$ all oscillators meet again with nearly identical phases, while in between two consecutive pulses each oscillator behaves independently, advancing its phase by exactly k clockwise round-trips, where k is the oscillator index. Note that this can be achieved in a trivial way already without coupling, i.e. $K = 0$. Indeed, starting with all phases initially identical, i.e. $\theta_k(0) = 0 \; \forall k$, for $K = 0$ the system will come back to this configuration after a period $T = 2\pi/\Delta\omega$. However, this trivial MLS has only neutral stability and all other trajectories are periodic with the same period but show less pronounced or no pulsations.
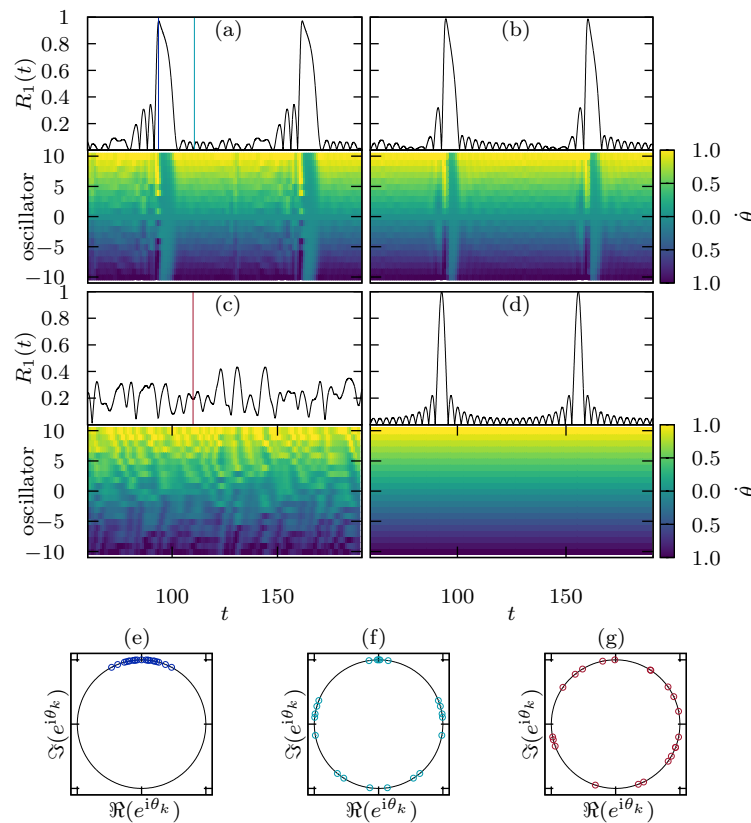

Figure 1: Numerically calculated solutions of system (1)–(2); (a)–(d): time evolution of mean field amplitude $R_1(t)$ and phase velocities $\dot{\theta}_k(t)$; (e)–(g): snapshots of the phases at the time moments indicated by vertical lines in (a) and (c). Parameter values: (a) $(K,\gamma)=(1.25, 0.7)$, (b) and (c) $(K,\gamma)=(0.91, 1.0)$, (d) $K=0$. The system size is $N=21$.

The basic mechanism for mode-locking is now that through the mean field coupling during the peak of $R_1(t)$ all oscillators are attracted towards the mean phase $\Psi_1(t)$ and in this way the pulsation becomes stable. Note that the coupling strength K has to remain below the synchronization threshold $K < K_C$ in order to avoid the onset of synchrony and to maintain the comb of effective frequencies.

In Fig. 1 we present numerically calculated solutions of system (1)–(2) for different parameter values and initial conditions. In panel (a) and (b) we show MLS with and without the second harmonic in the interaction function. It turns out that the solution $(K, \gamma){=}(1.25, 0.7)$ in panel (a) is globally stable, while the solution for $(K, \gamma){=}(0.91, 1.0)$, shown in panel (b), coexists with the state of phase turbulence shown in panel (c). In this case, the MLS can only be found for carefully prepared initial conditions, while the phase turbulence appears for random initial conditions. For comparison, we show the trivial MLS with $K{=}0$ in panel (d), where the phase relation for the pulses is set by the initial condition rather than developed dynamically. Panels (e)–(g) show time snapshots of the phases at the times indicated by colored vertical lines in panels (a) and (c), at the pulse, between the pulses, and in the turbulent regime, respectively. For the stable MLSs (a) and (b) the pulsation period is bigger than in the case of free rotation with natural frequencies (d), i.e. we find

$$\Delta\Omega < \Delta\omega.$$

The MLSs (a), (b) and (d) all carry the symmetry (4). The regime of phase turbulence for $(K, \gamma) = (0.91, 1)$, shown in panel (c), has already been reported in [3] where it is reported as the typical behavior of the system below synchronization, characterized by extensively chaotic Lyapunov spectra as shown in Fig. 2. Deep mathematical results on the stability of this state for random natural frequencies have been obtained only recently, see [11, 14]. MLSs in the Kuramoto model right below the synchronization threshold have been reported in [15] only for very small system size $N = 5$. Note that the fluctuations between two pulses in (b) are considerably smaller compared to the fluctuations in the turbulent regime (c). In [16] the mathematical framework for subharmonic locking of several oscillators in a more general setting has been elaborated.
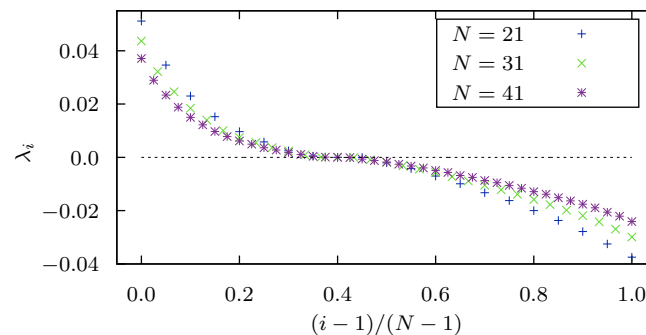

Figure 2: Lyapunov spectra for $(K, \gamma) = (0.91, 1)$ and different system sizes $N \in \{21, 31, 41\}$. The time span of the computation is $2 \cdot 10^5$ units.

3   Numerical methods

For all simulations we use a fourth order Runge-Kutta-method with a step size of $h = 0.01$. Since simulations of a flow on $\mathbb{T}^N$ are usually performed on the universal cover $\mathbb{R}^N$ one has to regularly project back to the unit circle interval in order to avoid digit cancellation in long simulations. To investigate MLSs we compute suitable Poincaré sections using the condition

$$\theta_k - \theta_{k+1} = 0 \tag{11}$$

for some $k \in -n, \ldots, n-1$. It is typically met once per pulse for a MLS, however, not necessarily close to the pulse itself. In parameter scans, where system parameters are changed adiabatically, we take care of possible numerical trapping in invariant subspaces induced by symmetry by adding small perturbations to the initial state after each adaption of the parameters. Lyapunov exponents are computed via continuous Gram-Schmidt orthonormalization procedure as it has been described in [17].

4   The role of first and second harmonics in the interaction function

As mentioned before, there is a fundamental difference between the case $\gamma = 1$ of only first harmonic in the interaction function and the case of a second harmonic added to the interaction function. For $\gamma = 1$, almost all initial conditions lead to the turbulent state and only specifically chosen initial conditions lead to a MLS. The presented solution have been obtained by choosing a fully synchronized solution found for $K > K_C$ as initial condition. Moreover, for $\gamma = 1$ the MLS is extremely fragile and sensitive to perturbations.

In contrast to that for suitably chosen γ the MLS solution is globally stable and can by found starting from random initial data. It turns out that the mode-locking mechanism is most efficient for $\gamma \approx 2/3$, where the interaction of oscillators with a phase difference $|\theta_j - \theta_k|\pi$ is particularly weak, cf. Fig. 3. Note that for $\gamma < 2/3$ there appears already a repulsive interaction of distant oscillators, forcing them towards an anti-phase position and in this way inhibiting the mode-locking mechanism.
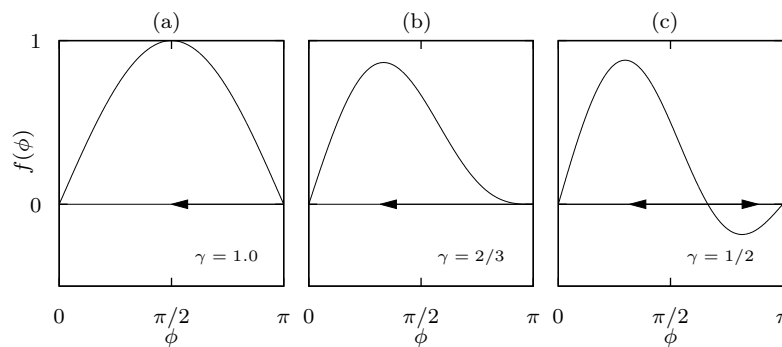

Figure 3: Interaction between two oscillators with phase difference ϕ for three different values of γ. For $2/3 \leq \gamma \leq 1$ the interaction is everywhere attractive, while for $\gamma < 2/3$ it becomes repulsive for $|\phi| \approx \pi$, attracting distant oscillators to an anti-phase position.

Another feature of the MLSs is the appearance of pulses in the second order parameter $R_2(t)$. They appear at the position of the pulse in the mean field $R_1(t)$ and additionally in the middle between two such pulses. Note that for the trivial case of $K = 0$ and $\theta_k(0)$ for all k (see Fig. 1(d)) we get $R_2(T/2) = 1$. During such intermediate pulses in $R_2(t)$ the second harmonic term in (7) dominates and the oscillators are attracted to the two anti-phase positions $\Psi_2(t)$ and $\Psi_2(t) + \pi$. It turns out that this process has a substantial impact on the stability of the MLS.

In Fig. 4 we compare the instantaneous stability along the MLS both for the case $(K, \gamma) = (0.91, 1.0)$, where the MLS coexists with phase turbulence and for the globally stable case at $(K, \gamma) = (1.25, 0.7)$. Together with the time traces of the order parameters we show the instantaneous expansion rate of

the phase space volume

$$\Lambda(t) = \sum_{i=1}^{N} \lambda_i(t) \tag{12}$$

given for each time t as the sum of the eigenvalues $\lambda_i(t)$ of the Jacobian along the MLS and the maximal instantaneous eigenvalue $\max \lambda_i(t)$. One can see in panel (a) that for $\gamma = 1$ there is a uniform level of volume expansion in between the pulses and only at the mode-locked pulse the expansion rate and eventually all instantaneous eigenvalues become negative. This is different for the case with second harmonic interaction, shown in panel (b). While in the first part of the inter pulse interval the stability properties are similar to the case of $\gamma = 1$, there appears another episode of volume contraction and instantaneous stability at the pulse in $R_2(t)$ and after this event the uniform level of volume expansion starts to disappear. In both cases, the stability of the MLS originates from a strong contraction during the pulse events, while over a large part of the period there is a volume expansion, inducing locally a growth of generic perturbations from the MLS. In the case with second harmonic interaction the contraction acts also during the pulse in $R_2(t)$ and in this way enhances substantially the stability and of the whole periodic orbit. In a similar way, additional higher harmonics could possibly have a further positive impact on the stability.
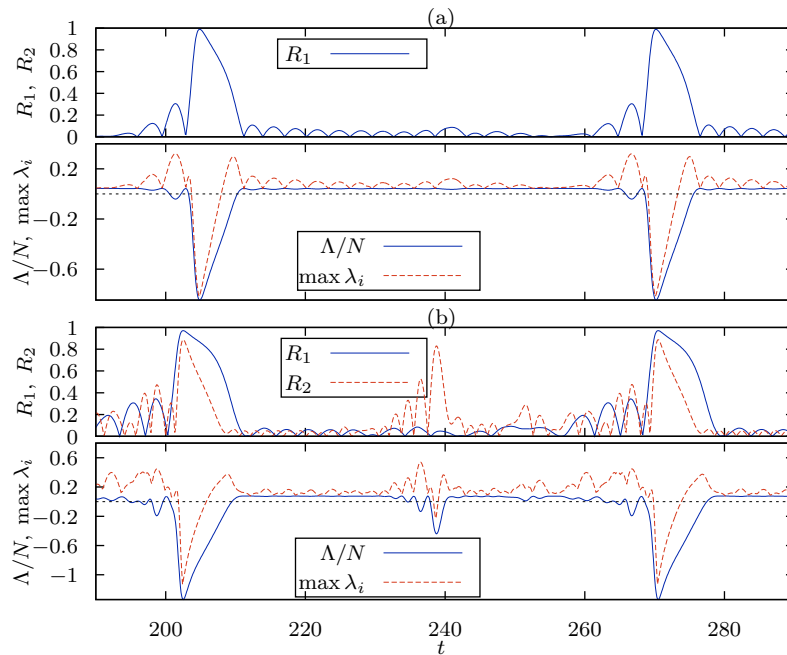

Figure 4: Time traces of order parameters $R_{1,2}$ (upper rows) together with normalized expansion rate of phase space volume $\Lambda(t)/N$ and maximal instantaneous eigenvalue $\max \lambda_i(t)$. Panel (a): MLS with first harmonic interaction $(K, \gamma) = (0.91, 1.0)$ (here only $R_1(t)$ is relevant); Panel (b): MLS with second harmonic interaction $(K, \gamma) = (1.25, 0.7)$.

5 Chaotic super-transients

Also for values of γ where the MLS are globally stable, they can be difficult to find in numerical simulations, because using random initial conditions the average transient time before the system reaches
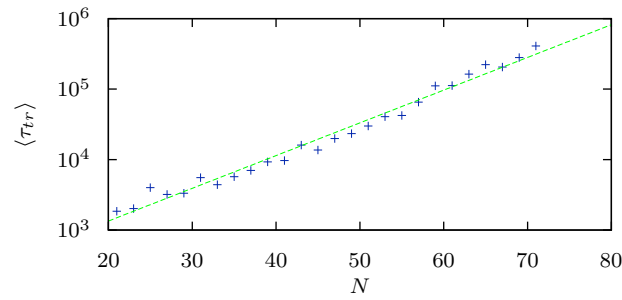
Figure 5: Logarithmic plot of the average transient time from random initial conditions to the stable MLS, varying the system size N. Averages are taken for $N \leq 53$ over 300 realizations of initial conditions. For larger N, their number had to be restricted to 50. Parameters: $(K, \gamma) = (1.2, 0.7)$.

a MLS increases drastically with the system size. Fig. 5 shows in a logarithmic plot the average transient time $\langle \tau_{\text{tr}} \rangle$ from random initial conditions to the stable MLS varying the system size N. At the chosen parameters $(K, \gamma) = (1.2, 0.7)$ all random initial data where found to converge to the MLS. Remarkably, we find that the average time spent on a chaotic transient, similar to the regime of phase turbulence observed for $\gamma = 1$, scales exponentially with the system size

$$\langle \tau_{\text{tr}} \rangle \propto e^{\kappa N}, \tag{13}$$

with the coefficient $\kappa \approx 0.11$. The transients can be classified as type-II chaotic super transients [18, 19], i.e. the transition from incoherence to the MLS is abrupt rather than gradually. Qualitatively, this scaling behavior can be explained by interpreting the nonlinear regime of phase turbulence as a random process, taking the phase configurations eventually into a certain small neighborhood of a MLS, where the linear stability dominates the nonlinear processes. The exponential scaling is then given by the average time that a random trajectory needs to reach a specific volume in $\mathbb{T}^N$, growing exponentially with N as well. The parameter γ in the interaction function has a substantial influence on the transient times. In Fig. 6 the average transient time in dependence of γ is shown for different system sizes N and coupling strengths K. Each points represent the average over 200 different initial conditions. The computations were stopped in the case of large periods as in modulated solutions and also when a transient exceeded 10^6 time units. Results are shown only for parameters, where a stable MLS was reached for all initial conditions within 10^6 time units. As we will see below, there are parameter values, where more complicated types of periodic solutions and multistability between them may exist. As γ increases, i.e for the first harmonic dominating, the transient times show an exponential growth before the MLS looses its stability.

6   Instabilities and bifurcations

Varying the parameters K and γ the stable MLSs can loose their stability and besides the phase chaos, one can observe a variety of more complicated solutions emerging from the fundamental MLS. In Fig. 7 a survey of the solutions for different parameter values is presented. The different levels of the order parameter, given in panel (a), allows to distinguish between synchrony (values close to one), phase chaos (intermediate values), and mode-locking (smallest values). The maximal values of the order parameter in panel (b) indicate the high coherence in the mode-locking peaks and allow to identify also those regions where such peaks appear erratically. Initial conditions are taken to be coherent that is the symmetric synchronous solution just above critical coupling $K > K_C$. Additionally a parameter scan is presented for $\gamma = 0.82$ in Fig. 8.
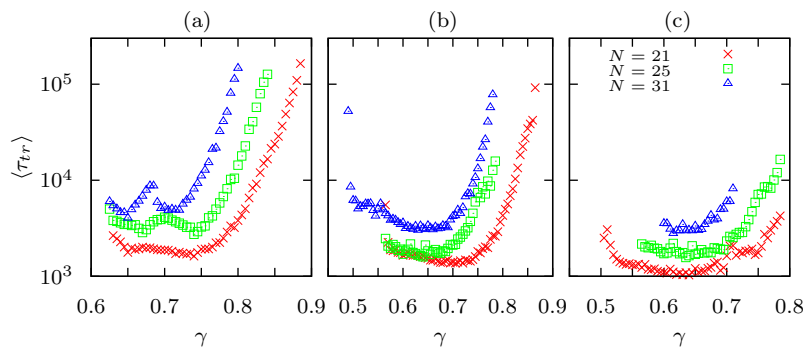
Figure 6: Average transient times in logarithmic plot for varying γ. Coupling strength $K = 1.2, 1.25, 1.3$, panels (a), (b), (c), respectively. Symbols/colors indicate different system sizes $N \in \{21, 25, 31\}$. Each point represents an average over 200 random initial condition.
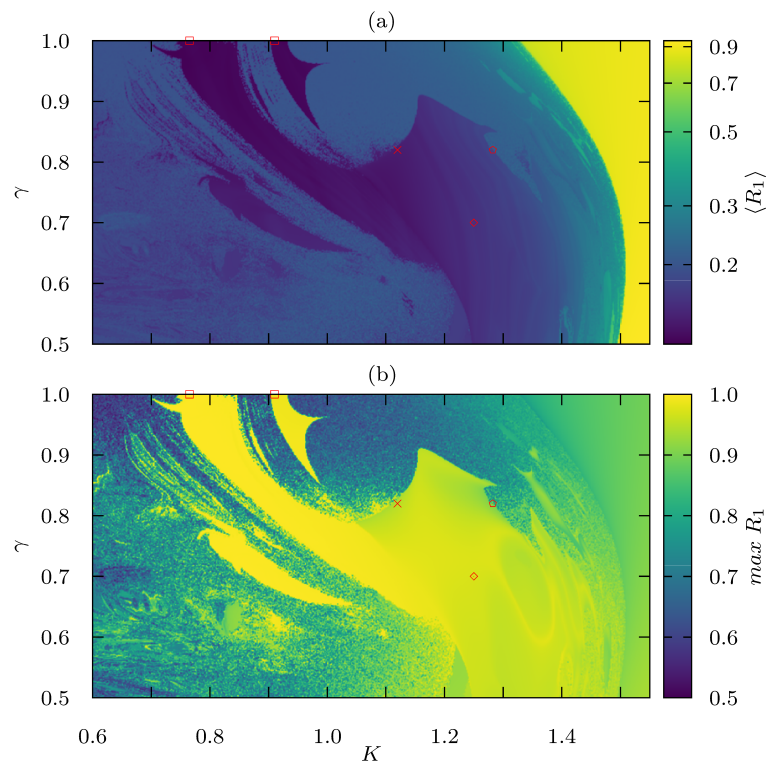

Figure 7: The average and maximal order parameter are shown in (a) and (b), respectively. The system size is $N = 21$ and market points indicate parameter values where solutions are presented in Fig. 1, 9, 10, and 11.
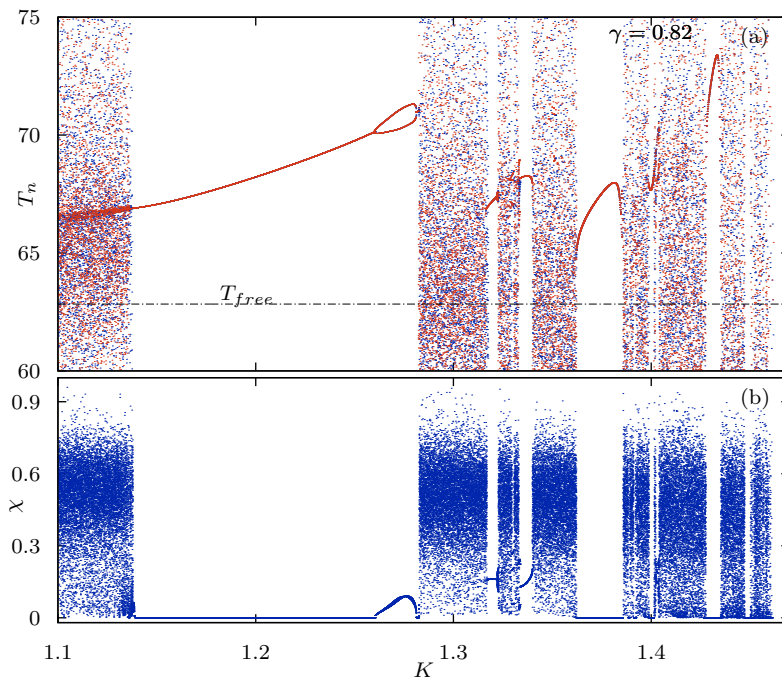
Figure 8: Panel (a): sampled return times for varying parameter K, $\gamma = 0.82$. Different colors correspond to increasing (blue) and decreasing (orange) coupling strength. Narrow periodic windows occur between regions of phase chaos. Panel (b): sampled distances χ from the symmetry invariant subspace with respect to the symmetry action σ at the crossings of the section.

6.1 Modulated mode-locked solutions

In the regime of fundamental mode-locking reappearing pulses are identical and the period is the time between two pulses. In addition, we observe solutions where the effective frequencies Ω_k are still equidistant, but the pulse heights and inter pulse intervals are modulated. This modulation can be periodic, quasi periodic, or chaotic. The transitions are mediated by period doubling or torus bifurcation resulting in periodic or quasi periodic modulation, respectively. Subsequently chaotically modulated MLSs can arise via torus break up or period doubling cascades.

6.2 Comb splitting

Another type of modulated solutions is observed when two different spacings between the effective frequencies appear, $\Omega_{k,k+1} \in \{\Delta\Omega_1, \Delta\Omega_2\}$. For two spacings with a rational relation $p\Delta\Omega_1 = q\Delta\Omega_2$ with $p, q \in \mathbb{N}$, we obtain a periodic solution with period

$$T = 2\pi p/\Delta\Omega_1 = 2\pi q/\Delta\Omega_2.$$

An example for first harmonic coupling $\gamma{=}1$ with a rational relation of the two spacings is shown in Fig. 9. From the evolution of $R_1(t)$, shown in panel (a), one can clearly see a modulation of the pulses. Consecutive inter pulse intervals obtained from the return times between crossings of the Poincaré section are plotted in panel (b). Note that the number of section crossings during a period with a split frequency comb depends on the frequency spacing between the two oscillators that are used for the section. In (c) we show the effective frequency spacings that are related here by the ratio $7/8$. When the ratio between the two spacings is irrational the solution has a quasi periodic modulation. In that case one finds a closed curve in the two dimensional Poincaré section instead of multiple points.
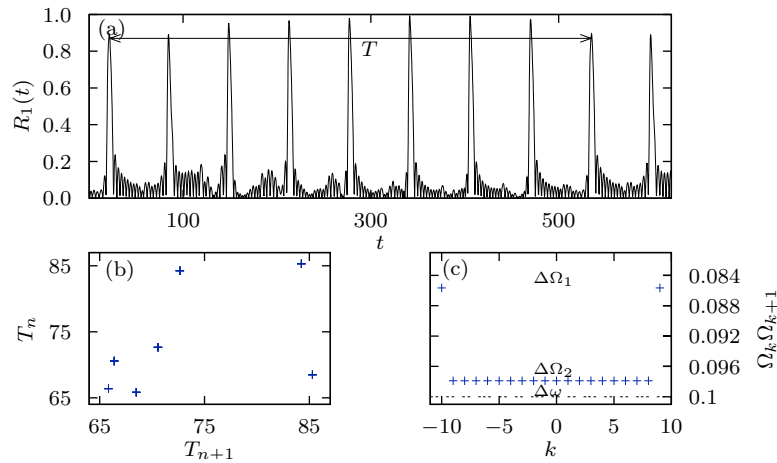
Figure 9: Comb splitting MLS for $(K, \gamma)=(0.765, 1.0)$ and $N = 21$. (a): time trace of the order parameter $R_1(t)$; (b): orbit of period 7 in a two dimensional Poincaré section with return times of consecutive section crossings plotted against each other; (c): spacings $\Delta\Omega$ of effective frequencies.

6.3 Torus breakup chaotically modulated MLS, symmetry breaking, and multistability

A scenario leading from a fundamental MLS towards more complicated solutions is shown in Fig. 10. A harmonic MLS undergoes a torus bifurcation with a subsequent breakup of the invariant torus and emergence of chaos In panel (a) we have sampled the Poincaré return times for varying coupling strength K, where the two different colors blue and orange correspond to sweeping in positive and negative direction, respectively. In a two dimensional Poincaré section, shown in panel (b), we observe the emergence of a closed curve. For further increasing K, this curve folds over and after the breakup of the corresponding invariant torus, a chaotic attractor appears, see panel (c). This chaotic attractor collapses via cascade of period doublings to a period five solution at slightly higher values of K, see panel (a). Here, two stable periodic solutions with five pulses per period coexist. These solutions do not have the symmetry (4) any more. Instead they show up as a symmetry related pair $\phi(t)$ and $\tilde{\phi}(t)$, satisfying

$$\phi_k(t) = -\tilde{\phi}_{-k}(t). \tag{14}$$

Since our Poincaré condition (11) is not invariant under the symmetry action (3), we get different return times for the $\phi(t)$ and $\tilde{\phi}(t)$, which can be distinguished by the two different colors in the period five window in panel (a). For further increasing K the period five orbit disappears in an intermittency transition as discussed in more detail in the next section.

6.4 Intermittency between phase turbulence and MLS

In addition to the transition from MLSs to low dimensional chaos as discussed above, we can also observe direct transitions to extensive chaos. This happens when a MLS or modulated MLS loses its stability and an intermittent behavior [20, 21] appears, alternating between phase chaos and episodes close to the weakly unstable MLS. As an example, we analyze the intermittent behavior in the parameter window below $K = 1.137$ for $\gamma = 0.82$. A time trace of $R_1(t)$ in this intermittent regime is shown in Fig. 11. It turns out that the two alternating regimes can be characterized by the rolling average of
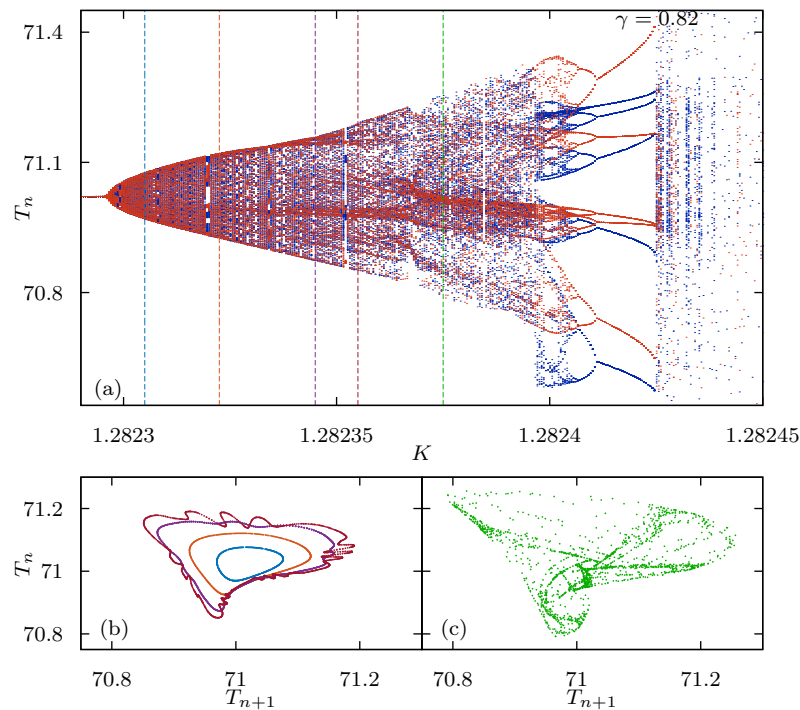
Figure 10: (a): Sampled return times T_n between crossings of the Poincaré section (11) for $\gamma = 0.82$ and varying K, blue and orange colors corresponds to sweeping K in increasing and decreasing direction. (b) and (c): two-dimensional representation of return times T_n for selected values of K given by dashed lines in panel (a). Closed curves in (b) represent invariant tori. Low dimensional chaos in (c).
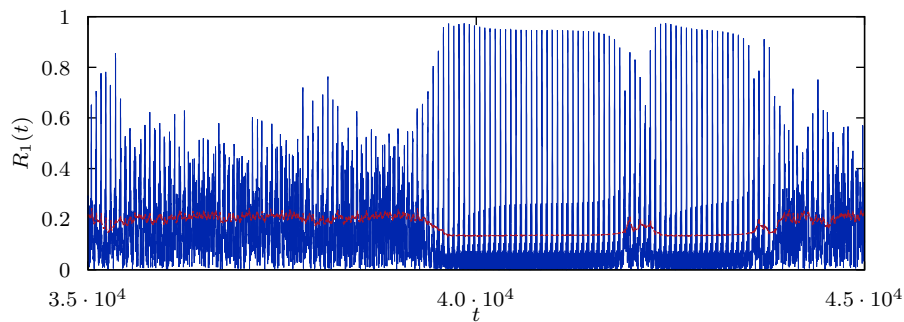

Figure 11: Time trace of $R_1(t)$ at $(K, \gamma) = (1.12, 0.82)$, showing intermittency between phase chaos and a MLS. The rolling average (15) can be used to distinguish between the two regimes (red line).

R_1 for a time window of length T close to the approximate inter pulse interval of the underlying MLS:

$$\langle R_1(t) \rangle_T = \frac{1}{T} \int_{t-T}^{t} R_1(\tau) d\tau. \tag{15}$$

This quantity, shown by the red line in Fig. 11, is almost constant when the system is close to the MLS and is fluctuating around a significantly higher value in the regime of phase chaos. In this way, we can extract from our numerical solutions the average fraction of mode-locking $\langle \tau \rangle_{\text{ML}}$ in the intermittent trajectories. Varying the coupling parameter close to its critical value we obtain a power law

$$\langle \tau \rangle_{\text{ML}} \propto |K - K_b|^{-\alpha}, \tag{16}$$

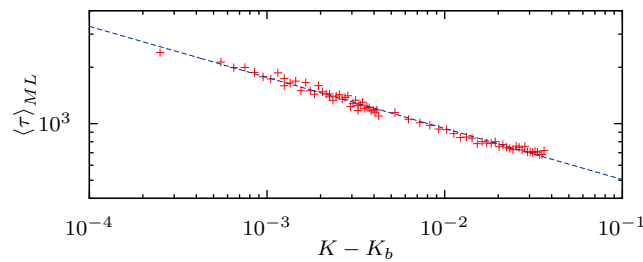where $K_b \approx 1.137$ is the bifurcation point and $\alpha \approx 0.27$, see Fig. 12.

Figure 12: Distance from the critical parameter K_b and average fraction of mode-locking $\langle \tau \rangle_{\text{ML}}$ in a double logarithmic plot.

7 Conclusion

We have introduced the notion of mode-locking for coupled phase oscillators and demonstrated this phenomenon in globally coupled systems of Kuramoto-Daido type with equidistant natural frequencies. Already below the Kuramoto-threshold this leads to a stable collective dynamical regime, characterized by sharp periodic pulses in the global mean field. Their stability can be substantially enhanced by introducing a second harmonic in the coupling function. In this case, for suitably chosen parameters the MLS is globally stable. For classical Kuramoto oscillators, i.e. with only the first harmonic in the coupling function they are difficult to find, since they can be found only in coexistence with stable phase chaos. Also in the cases where the MLS is globally stable, the transient times from random initial conditions to the MLS grow exponentially with the number of oscillators, while before this transition type-II supertransients of phase chaos are observed. In addition to the fundamental MLS, we demonstrate also the existence of various types of modulated MLSs and study the transitions between them. In particular, we observe an intermittent behavior between the extensive chaos of phase turbulence and the periodic regime of mode-locking.

References

[1] Y. Kuramoto, *Chemical Oscillations, Waves, and Turbulence*, (Springer Series in Synergetics, 1984).

[2] A. Pikovsky, M. Rosenblum and J. Kurths, *Synchronization: A Universal Concept in Nonlinear Sciences*, (Cambridge university press, Vol. 12., 2003).

[3] O. V. Popovych, Y. L. Maistrenko and P. A. Tass, Phys. Rev. E **71**, 065201(R) (2005).

[4] D. Pazó, Phys. Rev. E **72**, 046211 (2005).

[5] B. Ottino-Löffler and S. H. Strogatz, Phys. Rev. E **93**, 062220 (2016).

[6] H. A. Haus, Journal of Applied Physics **46**.7 (1975).

[7] A. G. Vladimirov and D. Turaev, Phys. Rev. A **72**, 033808 (2005).

[8] E. A. Avrutin, J. M. Arnold and J. H. Marsh, IEEE J. Sel. Top. Quantum Electron. **9**, 844 (2003).

[9] Y. H. Wen, M. R. E. Lamont, S. H. Strogatz and A. L. Gaeta, Phys. Rev. A **94**, 063843 (2016).

[10] D. Hansel, G. Mato and C. Meunier, Europhysics Letters (EPL) **23**.5 (1993): 367–72.

[11] H. Chiba and D. Pazó, Physica D: Nonlinear Phenomena **238**, 1068–1081 (2009).

[12] H. Daido, Physica D: Nonlinear Phenomena **91**, 24–66 (1996).

[13] M. Komarov and A. Pikovsky, Phys. Rev. Lett. **111**, 204101 (2013).

[14] H. Dietert, Journal de Mathématiques Pures et Appliquées **105**.4 (2016): 451–489.

[15] Y. L. Maistrenko, O. V. Popovych, O. Burylko and P. A. Tass, Phys. Rev. Lett. **93**, 084102 (2004).

[16] C. Baesens, J. Guckenheimer, S. Kim and R. Mackay, Physica D: Nonlinear Phenomena **49**, 387–475 (1991).

[17] F. Christiansen and H. H. Rugh, Nonlinearity **10**.5 (1997): 1063–072.

[18] C. Grebogi, E. Ott and J. A. Yorke, Ergodic Theory and Dynamical Systems **5**.03 (1985): 341–372.

[19] T. Tél and Y. C. Lai, Physics Reports **460**.6 (2008): 245–275.

[20] J. P. Eckmann, Reviews of Modern Physics, **53**(4), 643–655 (1981).

[21] Y. Pomeau and P. Manneville, Comm. Math. Phys. **74** (1980), no. 2, 189–197.